Letters

Time Domain Analysis of Reactive Components and Optimal Modulation for Isolated Dual Active Bridge DC/DC Converters

Shien Wang, *Student Member, IEEE*, Zedong Zheng, *Member, IEEE*, Chi Li, *Member, IEEE*, Kui Wang, *Member, IEEE*, and Yongdong Li, *Member, IEEE*

***Abstract*—This letter discusses the reactive components and the power factor of dual-active-bridge converters under triple-phase-shift modulation. Different from previous methods based on backflow power integral or Fourier series expansion, this letter presents a straightforward analysis and categories of reactive current through time domain analysis, and then gives a unified time domain definition of reactive current, reactive power, and power factor. Compared with all the previous definitions, the expressions of reactive components and power factor are much more concise and of a profound physical meaning. On this basis, specific calculations of reactive power and power factor are derived for all practical voltage patterns and an optimal global power factor phase shift modulation is proposed to improve the power factor on both bridges. At last, the effectiveness of analysis and proposed modulation were validated using a 500-W laboratory prototype. The results showed efficiency improvements compared to other optimal power factor modulation strategies.**

***Index Terms*—DC–DC power conversion, time domain analysis, optimal control, pulsewidth modulation.**

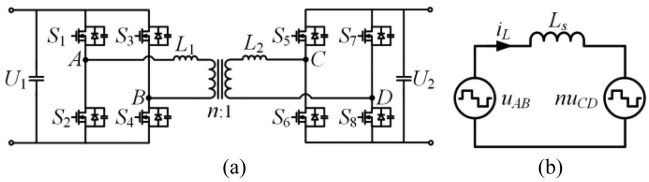

(a) (b)

I. Introduction

ISOLATED dual active bridge (DAB) converters are gaining more attention for the merits of simple structure, easy to control, and high power density. Single-phase-shift (SPS) modulation only utilizes the outer phase shift between high frequency (HF) voltages as control variable, and suffers huge HF current if the voltage gain is not matched with the high frequency transformer (HFT) turns ratio [1]. Numerous modulation strategies with more modulation parameters have been proposed in literatures to deal with this problem, such as extended-phase-shift (EPS) modulation in [2] and [3], dual-phase-shift (DPS) modulation in [4], and triple-phase-shift (TPS) modulation strategies for different optimization goals [5]–[8].

In order to study and quantify the effect of different modulation strategies, many works focused on the reactive power or the power factor in the HF link. Concept of reactive power was originally proposed in [4]. Based on this definition, the reactive power equals the flow back power and is generated by the phase different between the HF voltage and the HF current on primary bridge. However, the physical significance is not clear as the HF components are nonsinusoidal. The current stress was used to indicate the reactive power in [8], which lacked direct linking. Authors in [9]–[11] defined the reactive power

Manuscript received January 7, 2019; revised January 20, 2019; accepted January 28, 2019. Date of publication February 1, 2019; date of current version May 22, 2019. This work was supported by the National Key R&D Program of China under Grant 2017YFB1200901-12. *(Corresponding author: Zedong Zheng.)*

The authors are with the Department of Electrical Engineering, Tsinghua University, Beijing 100084, China (e-mail:

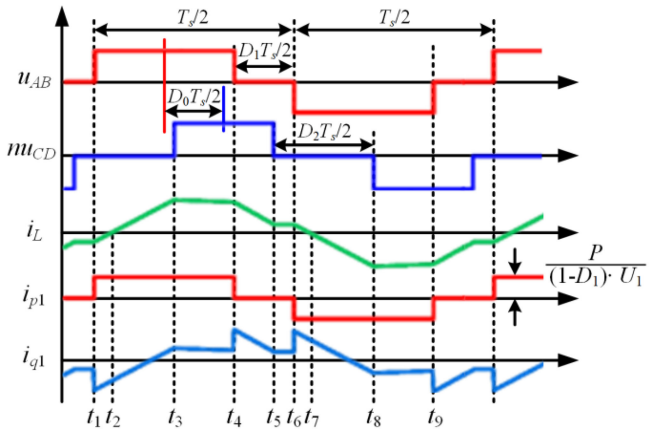

Fig. 2. Waveforms of HF voltages and HF currents for TPS modulation.

Fig. 2 shows the steady-state operation waveforms of TPS modulation. Power transfers from primary bridge to secondary bridge and equals *P*. The inner phase shift of the primary bridge is D_1, and u_{AB} is a square wave with duty cycle of $(1 - D_1)/2$. Similarly, the inner phase shift of the secondary bridge is D_2, and duty cycle of u_{CD} is $(1 - D_2)/2$. D_1 and D_2 are commonly limited within [0,1]. The outer phase shift between u_{AB} and u_{CD} is D_0, and is generally limited within $[-0.5, 0.5]$. All the phase shift parameters have influences on the HF current i_L and power transfer characteristics, but the magnitude and the current stress of i_L can be reduced through appropriate combinations. The voltage gain *M* and root-mean-square value of HF components are defined as

$$M = \frac{nU_2}{U_1}, \quad U_{AB} = \mathrm{RMS}\left(u_{AB}\right) = U_1\sqrt{1-D_1}$$
$$I_L = \mathrm{RMS}\left(i_L\right), \quad U_{CD} = \mathrm{RMS}\left(u_{CD}\right) = U_2\sqrt{1-D_2}. \tag{1}$$

B. Time Domain Analysis of Reactive Current

In Fig. 2, the instant power is negative between t_1 and t_2 or between t_6 and t_7, so i_L during this time interval was usually defined as the circling current and the power during this time interval was defined as the reactive power in [4] and [5]. However, this definition is narrow to depict the influence of voltage mismatch and phase shift modulation, so a new analysis of the reactive current is proposed.

u_{AB} keeps zero from t_4 to t_6, and the primary bridge cannot provide any active power during this time interval. However, i_L is not always equal to zero from t_4 to t_6. Thus, i_L does not transfer any power from primary bridge but still causes conduction losses. So this part of i_L is defined as the freewheeling reactive current.

u_{AB} equals U_1 from t_1 to t_4, and the primary bridge transfers power during this time interval. The average value of i_L between t_1 and t_4 is

$$I_{\mathrm{ave1}} = \frac{P}{(1-D_1)U_1}. \tag{2}$$

If i_L is ideally even and equals I_{ave1} between t_1 and t_4, the converter can transfer the same amount of power with the minimum current stress and current rms value. The rest part of i_{L} during this interval fluctuates around zero and does not transfer active power but increases both conduction and switching losses. Thus, it is defined as the fluctuant reactive current. It is worth mentioning that the circling current is included in the fluctuant reactive current.

Based on analysis above, the ideal current for primary bridge should have the same shape as u_{AB}, as i_{p1} shown in Fig. 2. Generally, i_{p1} transfers the same amount of power as i_L, but with the minimum rms value and current stress, and is defined as the active part of i_L. The expression of i_{p1} and its rms value are

$$i_{p1} = \frac{P}{{U_{AB}}^2}u_{AB}, \; I_{p1} = \mathrm{RMS}\left(i_{p1}\right) = \frac{P}{U_{AB}}. \tag{3}$$

The rest part of i_L contains freewheeling reactive current and fluctuate reactive current, and is the overall reactive current of the primary bridge

$$i_{q1} = i_L - i_{p1}, \; I_{q1} = \mathrm{RMS}\left(i_{q1}\right) = \sqrt{I_L^2 - I_{p1}^2}. \tag{4}$$

i_{p1} and i_{q1} are orthogonal in the switching period

$$\begin{aligned}\frac{1}{T}\int_0^T i_{p1}i_{q1}\,dt &= \frac{1}{T}\int_0^T i_{p1}\left(i_L - i_{p1}\right)dt \\ &= \frac{P}{\left(1-D_1\right){U_1}^2 T}\int_0^T u_{AB}\,i_L\,dt - I_{p1}^2 \\ &= \frac{P^2}{\left(1-D_1\right){U_1}^2} - \frac{P^2}{\left(1-D_1\right){U_1}^2} = 0.\end{aligned} \tag{5}$$

Similar analysis can be done to obtain the active current and the reactive current of the secondary bridge with variables referred to the primary side

$$i_{p2} = \frac{P}{nU_{CD}^2}u_{CD}, \; I_{p2} = \mathrm{RMS}\left(i_{p2}\right) = \frac{P}{nU_{CD}} \tag{6}$$

$$i_{q2} = i_L - i_{p2}, \; I_{q2} = \mathrm{RMS}\left(i_{q2}\right) = \sqrt{I_L^2 - I_{p2}^2}. \tag{7}$$

C. Definition of Reactive Power and Power Factor

Since i_{p1} and i_{q1} are orthogonal, the reactive power, the apparent power, and the power factor of primary bridge are

$$Q_1 = U_{AB}\cdot I_{q1} \tag{8}$$

$$S_1 = \sqrt{P^2 + {Q_1}^2} = U_{AB}\cdot\sqrt{I_{p1}^2 + I_{q1}^2} = U_{AB}\cdot I_L \tag{9}$$

$$\lambda_1 = \frac{P}{S_1} = \frac{P}{U_{AB}\cdot I_L}. \tag{10}$$

Note that (8)–(10) are the same as the summations of infinite series from frequency domain analysis in [9]–[11] and accord with the definitions for nonsinusoidal single-phase systems [12]. However, the physical meaning and expressions are much more straightforward with the concept of reactive current through time domain analysis. Similar analysis can be done to obtain the power factor of the secondary bridge as

$$\lambda_2 = \frac{P}{S_2} = \frac{P}{nU_{CD}\cdot I_L}. \tag{11}$$

Since the primary bridge and the secondary bridge are equally important in the power transfer, the global power factor is defined to quantify the effectiveness of modulation strategies

$$\begin{aligned}\lambda_{12} = \lambda_1\lambda_2 &= \frac{P^2}{nU_{AB}U_{CD}I_L^2} \\ &= \frac{P^2}{nU_1U_2I_L^2\sqrt{\left(1-D_1\right)\left(1-D_2\right)}}.\end{aligned} \tag{12}$$

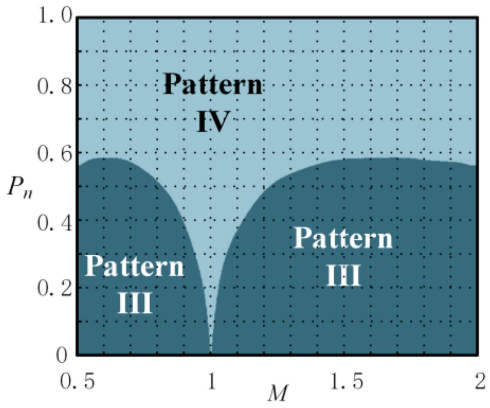

Fig. 3. Optimized voltage pattern operation area.

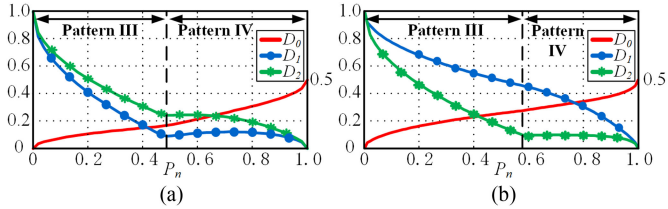

Fig. 4. Modulation curves of OGPF for (a) $M = 1.2$ and (b) $M = 0.6$.

III. Optimal Modulation Scheme

In this section, specific expression of λ_{12} is derived for different voltage patterns. Then an optimal global power factor (OGPF) modulation is proposed to operate DAB with the maximal λ_{12}. To simplify the analysis, only modulation parameters for forward power flow is calculated.

A. Optimization Based on Voltage Patterns

According to [5], the operation of DAB converter can be classified into 12 voltage patterns depend on the relationships between modulation parameters, but only four of them are practical for forward power flow [7]. The following base values are used to normalize state variables:

$$U_B = U_1, P_B = \frac{nU_1U_2}{8f_sL_s}, I_B = \frac{nU_2}{8f_sL_s}, Z_B = \frac{8f_sL_s}{M}. \quad (13)$$

As studied in [5] and [7], normalized I_L and normalized P are derived for each voltage pattern, as listed in (A.1) and Table I in the appendix. Take (A.1) and Table I into (12), expression of λ_{12} for each voltage patterns can be obtained. Then for certain P and M, the optimization problem to maximize λ_{12} can be solved within constraints determined by voltage pattern conditions and transferred power. Compare and synthesize the results of all the voltage patterns, the optimal modulation parameters for OGPF modulation can be derived.

Fig. 3 presents the optimization results of the voltage pattern operation area. As proved in [8], Patterns I and II can be mapped into Pattern III with smaller I_L, so they disappear in the optimized operation area. Pattern III is adopted for light load conditions and Pattern IV is used for heavy load conditions.

Fig. 4 shows the OGPF modulation curves for different M. D_0 increases from 0 to 0.5 while D_1 and D_2 decrease from 1 to 0 with increase in active power. When $M > 1$, D_1 is always smaller than D_2, whereas D_2 is smaller when $M < 1$. With a greater voltage mismatch (i.e., $M = 0.6$), larger inner phase shifts are required to improve the global power factor.

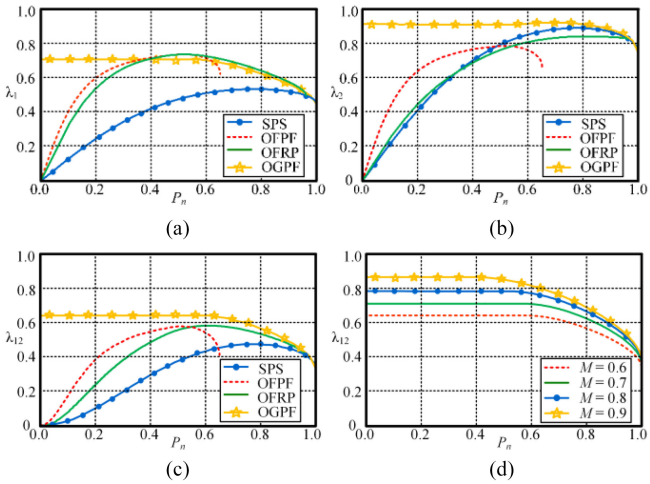

Fig. 5. Comparison of power factor. (a) λ_1 of different modulation strategies. (b) λ_2 of different modulation strategies. (c) λ_{12} of different modulation strategies. (d) λ_{12} of OGPF modulation with different M.

Fig. 5(a)–(c) presents the power factor of different modulation strategies, including SPS modulation, optimal fundamental power factor (OFPF) modulation in [9], optimal fundamental reactive power (OFRP) modulation in [10], and OGPF modulation. SPS modulation provides the lowest global power factor under most load conditions, but is able to cover the whole power range. OFPF modulation operates high λ_1 at light load conditions but covers the least power range. OFRP modulation provides high λ_1 under heavy load and covers larger power range than OFPF modulation. OFPF modulation and OFRP modulation are special cases of EPS modulation, where the duty ratio of the low voltage bridge is kept 50% even under light loads. So there is great fluctuant reactive current under light load condition and results in near zero power factor. OGPF modulation does not possess the highest λ_1 under all load conditions, but owns the highest λ_2 and λ_{12}. With OGPF modulation, the duty cycles of HF voltages are close to zero when the output power approaches zero, thus, i_L is reduced and the power factor is still kept high. Fig. 5(d) shows the power factor of OGPF modulation for different M. The power factor is always lower with larger voltage mismatches, especially under light loads.

B. Experiment Results

A prototype was built to verify the theoretical analysis. The equivalent inductance was 27.4 μH, the turns ratio of HFT was 1:1, and f_s was 40 kHz. The input dc voltage varied between 60–90 V, and the reference output voltage was set 75 V.

For digital implementation of OGPF modulation, D_1 and D_2 with different D_0 and M were precalculated and stored in a look up table. The input dc voltage and the output dc voltage were sampled, and a PI regulator took the output error to obtain D_0. Then linear interpolation was used to derive D_1 and D_2 from the look up table with output D_0 and instant M.

Figs. 6 and 7 show the experimental waveforms of OGPF modulation. The inner phase shift of high voltage bridge was larger to improve the power factor.

Fig. 8 shows the measured efficiency of different modulation strategies. OGPF modulation provided the highest efficiency for most power

TABLE I
NORMALIZED ACTIVE POWER AND THE REMAINDER TERM OF DIFFERENT VOLTAGE PATTERNS

No.	Conditions	Normalized active power P_n and e_{rmd}	Range of P_n
I	$0 < D_0 < (D_2 - D_1)/2$	$P_{I,n} = 4(1-D_2)D_0$, $e_{rmd,I} = (1-D_2)(2-12D_0^2-3D_1^2-D_2^2+2D_2)$	$[0, 0.5]$
II	$0 < D_0 < (D_1 - D_2)/2$	$P_{II,n} = 4(1-D_1)D_0$, $e_{rmd,II} = (1-D_1)(2-12D_0^2-3D_2^2-D_1^2+2D_1)$	$[0, 0.5]$
III	$\frac{\lvert D_2 - D_1\rvert}{2} < D_0 < \min\left[\frac{D_1+D_2}{2}, 1-\frac{D_1+D_2}{2}\right]$	$P_{III,n} = -2D_0^2 + 4D_0 - 2D_0(D_1+D_2) - 0.5\cdot(D_1-D_2)^2$ $e_{rmd,III} = 0.5\cdot(2D_0+D_1+D_2)^3 - 12D_0D_1D_2 - 12D_0^2 - 3D_1^2 - 3D_2^2 + 2$	$\left[0, \frac{2}{3}\right]$
IV	$(D_1+D_2)/2 < D_0 < 1-(D_1+D_2)/2$	$P_{IV,n} = 4D_0(1-D_0) - D_1^2 - D_2^2$ $e_{rmd,IV} = (1-2D_0)(2-4D_0^2-3D_1^2-3D_2^2+4D_0)$	$[0, 1]$

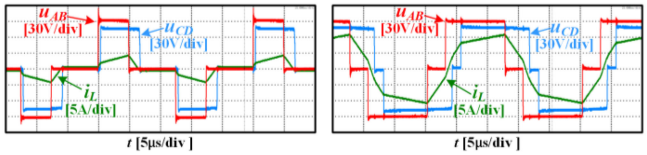

Fig. 6. Waveforms with $U_1 = 90$ V and $U_2 = 75$ V. (a) P = 100 W. (b) P = 500 W.

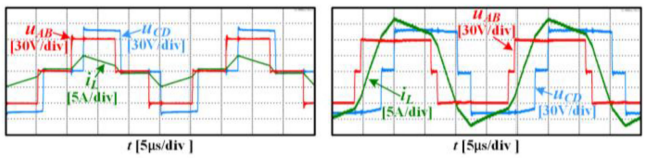

Fig. 7. Waveforms with $U_1 = 60$ V and $U_2 = 75$ V. (a) $P = 100$ W. (b) $P = 500$ W.

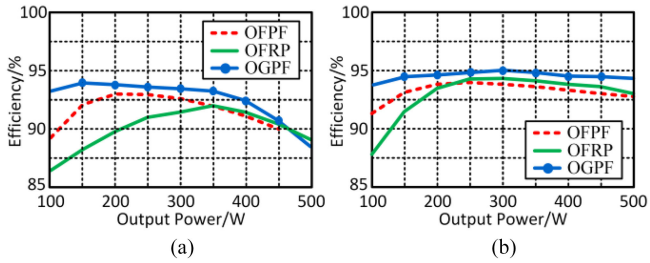

Fig. 8. Measured efficiency with $U_2 = 75$ V. (a) $U_1 = 60$ V. (b) $U_1 = 90$ V.

load. Compared to OFRP modulation, efficiency of OFPF modulation was higher under light loads but lower under heavy loads, which accords to the tendency of power factor in Fig. 5.

IV. CONCLUSION

With time domain analysis, reactive current can be divided into freewheeling reactive current and fluctuant reactive current. With that, reactive power and power factor are defined in time domain with a profound physical meaning, and their specific expressions are derived with a concise form. An optimal global power factor modulation strategy is proposed, which can provide the highest global power factor and cover the whole power range. This method can also be adopted for other isolated DC-DC converters to achieve high power factor power transfer.

APPENDIX

The normalized I_L and P for different voltage patterns are derived, where e_{rmd} is the remainder term and is different for each voltage pattern. Detailed derivation can be found in [5] and [7]

$$I_{L,n} = \sqrt{\frac{4}{3M^2}\left(1-3D_1{}^2+2D_1{}^3\right)+\frac{4}{3}\left(1-3D_2{}^2+2D_2{}^3\right)-\frac{4}{3M}e_{\mathrm{rmd}}}. \tag{A.1}$$

REFERENCES

[1] Y. Xie, J. Sun, and J. S. Freudenberg, "Power flow characterization of a bidirectional galvanically isolated high-power DC/DC converter over a wide operating range," *IEEE Trans. Power Electron.*, vol. 25, no. 1, pp. 54–66, Jan. 2010.

[2] B. Zhao, Q. Yu, and W. Sun, "Extended-phase-shift control of isolated bidirectional DC–DC converter for power distribution in microgrid," *IEEE Trans. Power Electron.*, vol. 27, no. 11, pp. 4667–4680, Nov. 2012.

[3] V. Karthikeyan and R. Gupta, "Zero circulating current modulation for isolated bidirectional dual-active-bridge DC–DC converter," *IET Power Electron.*, vol. 9, no. 7, pp. 1553–1561, 2016.

[4] H. Bai and C. Mi, "Eliminate reactive power and increase system efficiency of isolated bidirectional dual-active-bridge DC–DC converters using novel dual-phase-shift control," *IEEE Trans. Power Electron.*, vol. 23, no. 6, pp. 2905–2914, Nov. 2008.

[5] F. Krismer and J. W. Kolar, "Closed form solution for minimum conduction loss modulation of DAB converters," *IEEE Trans. Power Electron.*, vol. 27, no. 1, pp. 174–188, Jan. 2012.

[6] J. Huang, Y. Wang, Z. Li, and W. Lei, "Unified triple-phase-shift control to minimize current stress and achieve full soft-switching of isolated bidirectional DC–DC converter," *IEEE Trans. Ind. Electron.*, vol. 63, no. 7, pp. 4169–4179, Jul. 2016.

[7] A. Tong, L. Hang, G. Li, X. Jiang, and S. Gao, "Modeling and analysis of a dual-active-bridge-isolated bidirectional DC/DC converter to minimize rms current with whole operating range," *IEEE Trans. Power Electron.*, vol. 33, no. 6, pp. 5302–5316, Jun. 2018.

[8] S. Shao, M. Jiang, W. Ye, Y. Li, J. Zhang, and K. Sheng, "Optimal phase shift control to minimize reactive power for a dual active bridge DC-DC converter," *IEEE Trans. Power Electron.*, to be published.

[9] B. Zhao, Q. Song, W. Liu, G. Liu, and Y. Zhao, "Universal high-frequency-link characterization and practical fundamental-optimal strategy for dual-active-bridge DC-DC converter under PWM plus phase-shift control," *IEEE Trans. Power Electron.*, vol. 30, no. 12, pp. 6488–6494, Dec. 2015.

[10] H. Shi, H. Wen, J. Chen, Y. Hu, L. Jiang, and G. Chen, "Minimum-reactive-power scheme of dual-active-bridge DC–DC converter with three-level modulated phase-shift control," *IEEE Trans. Ind. Appl.*, vol. 53, no. 6, pp. 5573–5586, Nov./Dec. 2017.

[11] H. Shi, H. Wen, Y. Hu, and L. Jiang, "Reactive power minimization in bidirectional DC–DC converters using a unified-phasor-based particle swarm optimization," *IEEE Trans. Power Electron.*, vol. 33, no. 12, pp. 10990–11006, Dec. 2018.

[12] *IEEE Standard Definitions for the Measurement of Electric Power Quantities Under Sinusoidal, Nonsinusoidal, Balanced, or Unbalanced Conditions*, IEEE Standard 1459-2010 (Revision IEEE Standard 1459-2000), Mar. 2010, pp. 1–50.